

Influence of hydrogen core force shielding on dislocation junctions in iron

Haiyang Yu,^{1,*} Ivaylo H. Katsarov^{1,2,3,†} Anthony T. Paxton,^{2,‡} Alan C. F. Cocks^{1,4,§} and Edmund Tarleton^{1,4,||}

¹Department of Materials, University of Oxford, Parks Road, OX1 3PH, United Kingdom

²Department of Physics, King's College London, Strand, London WC2R 2LS, United Kingdom

³Bulgarian Academy of Sciences, Institute of Metal Science, 67 Shipchenski Prohod, 1574 Sofia, Bulgaria

⁴Department of Engineering Science, University of Oxford, Parks Road, OX1 3PJ, United Kingdom



(Received 23 December 2019; revised manuscript received 26 February 2020; accepted 6 March 2020; published 30 March 2020)

The influence of hydrogen on dislocation junctions has been analyzed by incorporating a hydrogen-dependent core force into nodal-based discrete dislocation plasticity simulations. Hydrogen reduces the core energy of dislocations, which reduces the magnitude of the dislocation core force. We refer to this as *hydrogen core force shielding*, as it is analogous to hydrogen elastic shielding but occurs at much lower hydrogen concentrations. The dislocation core energy change due to hydrogen was calibrated at the atomic scale, accounting for the nonlinear interatomic interactions at the dislocation core, giving the model a sound physical basis. Hydrogen was found to strengthen binary junctions and promote the nucleation of dislocations from triple junctions. Simulations of microcantilever bend tests showed hydrogen core force shielding reduced the yield stress followed by increased strain hardening due to junction strengthening. These simulations demonstrate hydrogen effects at a small bulk hydrogen concentration, 10 appm, realistic for body-centered cubic iron, allowing micromechanical tests on hydrogen charged samples to be simulated.

DOI: [10.1103/PhysRevMaterials.4.033607](https://doi.org/10.1103/PhysRevMaterials.4.033607)

I. INTRODUCTION

Understanding the effect of hydrogen on dislocations [1] is essential to understanding how hydrogen reduces ductility in metals. Using *in situ* TEM testing, hydrogen has been observed to enhance dislocation mobility in a variety of materials [2–4]. Ferreira *et al.* [5] found that hydrogen decreases the equilibrium dislocation spacing in a pileup in 310 stainless steel and Al. The same authors then observed that hydrogen suppresses dislocation cross slip, thereby increasing slip planarity [6]. Motivated by these experimental observations, Birnbaum and Sofronis [7] used analytic solutions to calculate the elastic stress field generated by a hydrogen concentration field that is in equilibrium with an edge dislocation (assuming plane strain). The elastic interaction between two dislocations or between a dislocation and a center of dilation (defect) is reduced in the presence of hydrogen, leading to reduced spacing and enhanced mobility. This mechanism is able to partially account for the experimental observation of hydrogen enhanced plasticity and is referred to as the hydrogen elastic shielding mechanism. Based on this mechanism, the effects of hydrogen on dislocation nucleation (Frank-Read source operation), expansion, and cross slip have been discussed [8]. These theoretical studies focused on dislocation behavior limited to a single slip plane and considered only the long-range elastic

stress, which is important for dislocation glide, but neglected the details of the dislocation core. Consequently, a very high bulk hydrogen concentration, typically $>10^4$ appm [7], has to be applied to observe any effect of hydrogen through the hydrogen elastic shielding mechanism. High concentrations are possible in face-centered cubic (fcc) materials, but because of the very low solubility of hydrogen in body-centered cubic (bcc) materials such as iron, typical hydrogen concentrations range between 1 and 10 appm in industrial applications and up to 100 appm in laboratory charged specimens, and at these concentrations elastic shielding is negligible. We propose here that in body-centered cubic (bcc) metals, hydrogen influences plasticity by reducing the dislocation core energy, which reduces the dislocation core force. The effects are very similar to reducing the elastic stress field but they occur at the low concentrations typical in bcc metals.

A sessile junction forms when a glissile dislocation cuts through a forest dislocation. This mechanism contributes to the formation of complex, tangled dislocation arrays during crystal deformation [9] and is a key source of strain hardening. Given their importance, dislocation junctions have been extensively studied [10]. Transmission electron microscopy (TEM) observations of dislocation structures of hydrogen-charged specimens in bcc Fe show that a homogeneous dislocation forest in a hydrogen-free sample transforms into cell walls that partition dislocation-free regions when it is charged with hydrogen. The cell walls can be regarded as dense dislocation tangles. TEM images reveal that the area of the dislocation-free zones and the density in the dislocation tangles increase with hydrogen concentration in the interval 0–25 appm [11]. The physics underlying dislocation reorganization due to hydrogen is not yet well established, but investigations into the

*haiyang.yu@materials.ox.ac.uk

†ivaylo.katsarov@kcl.ac.uk

‡tony.paxton@kcl.ac.uk

§alan.cocks@eng.ox.ac.uk

||edmund.tarleton@eng.ox.ac.uk

effect of hydrogen on dislocation junctions provide a useful starting point for understanding this phenomenon.

It is instructive to observe a single dislocation junction and study its formation and destruction. This will help predict and understand the emergent properties of dislocation tangles. Because of the difficulty in pinpointing and following the development of a single junction, only a handful of experimental observations have been reported in the literature [12–15]. This research investigated the formation and destruction of Lomer junctions using TEM, in the absence of hydrogen. Experimental investigation becomes even more challenging when hydrogen is present. Conditions apart from the hydrogen concentration ought to be equivalent between the charged and uncharged experiments, including the initial configuration of the junction (strictly speaking), its surrounding dislocation structure, and the loading history. Because of the statistical nature of dislocation activity, exact comparison between hydrogen charged and unchanged specimens is out of the question. Even for *in situ* tests, it is extremely difficult, if not impossible, to keep all the control variables unchanged. For instance, hydrogen charging will inevitably alter the dislocation structure, and the loading history will be distinct for different tests. No experimental observations on the effect of hydrogen on junctions have been reported for individual dislocation junctions, and it is questionable whether this will be achieved in the near future.

In the absence of suitable experiments, modeling can provide detailed and important information about the development of junctions and how they influence cell formation. Molecular dynamics (MD) [16] and three-dimensional (3D) discrete dislocation dynamics (DDD) [17] are powerful tools for simulating dislocation junctions. Rodney and Phillips [18] employed the quasicontinuum (QC) method, which combines MD and the finite element method (FEM), to study the formation and destruction of Lomer-Cottrell junctions. Bulatov *et al.* and Yamakov *et al.* [16,19] simulated Lomer-Cottrell junctions using molecular dynamics simulation. Molecular statics simulation can also be used to simulate dislocation locks [20,21]. Atomistic methods are limited to small temporal and spatial scales, compromising their ability to capture the long-range character of dislocation stress fields [22]; in general, the results obtained via atomistic methods cannot be directly implemented in large-scale (e.g., crystal plasticity) models. DDD is an ideal tool for bridging the gap in space and timescales between atomistic and continuum models. DDD has a dislocation line segment as its basic element and uses analytic solutions for the elastic fields so is able to simulate the collective behavior of a large array of dislocations. To date, DDD has been used to study problems ranging from individual dislocation junctions [23] to large-scale plasticity arising from the motion of a large number of dislocations [24]. Shenoy *et al.* [25] performed DDD simulations of a Lomer-Cottrell junction, reproducing the atomistic results obtained by Rodney and Phillips [18]. Madec *et al.* [23] performed systematic DDD simulations of Lomer-Cottrell junctions covering all possible initial configurations, and further evaluated the effect of forest hardening on plasticity using large-scale DDD simulations. Madec *et al.* [21] utilized the DDD approach in combination with molecular statics simulations to study the collinear interaction of dislocations. Bulatov *et al.* [10]

probed the properties of multijunctions using DDD and Lee *et al.* [26] performed DDD simulations of Lomer junctions in a free-standing thin film. Wu *et al.* [27] studied binary junctions in hexagonal close-packed crystals, combining the line tension model and DD simulations. Good agreement with the experimental observations was obtained [10,23], verifying the utility of DDD for simulating dislocation junctions.

Despite the large literature on modeling the effects of hydrogen on mechanical properties, across a wide range of scales, very few have investigated the effect of hydrogen on dislocation junctions. Hoagland and Baskes [28] studied the effects of hydrogen on a Lomer-Cottrell lock using Monte Carlo (MC) calculations. Chen *et al.* [29] investigated the effects of a general solute on a Lomer junction, considering different solute properties, using a kinetic Monte Carlo (kMC) coupled DDD approach. Hydrogen redistribution during the destruction of the dislocation junction was not considered in these works. Recently, Yu *et al.* [30] utilized a hydrogen informed discrete dislocation dynamics (DDD) approach to investigate the influence of hydrogen on Lomer junctions; hydrogen redistribution was taken into account and various initial configurations [23] were examined. This could provide a reference for modeling hydrogen with a crystal plasticity approach which considers dislocation interactions [31]. Zhao *et al.* [32] performed MD simulations of a hydrogen charged nanoindentation test and discussed the effect of hydrogen on dislocation entanglement.

Recently, Gu and El-Awady [33] proposed a framework for incorporating hydrogen into the nonsingular DDD formulation [34]. Hydrogen is treated as an isotropic point dilatation in an infinite elastic medium, based on which the hydrogen elastic stress field and its influence on dislocation motion are evaluated. This formulation accounts only for the linear elastic contribution of hydrogen residing outside the dislocation core region, which is consistent with the hydrogen elastic shielding mechanism. Similar formulations were also proposed in two dimensions (2D) [35,36]. However, this is only a partial contribution of hydrogen. Considering only the elastic shielding effect showed no influence of hydrogen at a realistic bulk hydrogen concentration (≤ 10 appm) [37].

As described by the hydrogen elastic shielding theory, hydrogen forms atmospheres around dislocations, reducing the long-range elastic dislocation-dislocation interactions [7,33]. At high hydrogen concentrations, the hydrogen shielding effect increases, which could affect the formation of dislocation structures. Although the elastic shielding effect is often quoted in the literature as a viable explanation for the reduction of elastic interactions between dislocations, at realistic bulk hydrogen concentrations it is unable to explain experimental observations of hydrogen-induced softening, for instance, in Ref. [38], where apparent softening in the loading curve was observed in a microcantilever test. Theoretical studies using continuum models show that the hydrogen shielding effect is relatively short ranged and unlikely unless hydrogen concentrations are extremely high ($> 10^4$ appm) [7]. Experiments using *in situ* TEM on samples deformed in tension [5] also show that hydrogen has a significant effect on dislocation spacing at distances greater than 20 b, indicating that hydrogen elastic shielding of the dislocation-dislocation interactions cannot, by itself, account for the observations. Atomistic simulations of

the effects of hydrogen on $1/2\langle 111 \rangle$ edge dislocation pileups in bcc Fe also indicate that the shielding mechanism is not operative at hydrogen concentrations lower than 10^5 appm [39]. Thus, other mechanisms, such as hydrogen binding in the dislocation core must be examined in more detail.

To account for the hydrogen core contribution, Yu *et al.* [37] implemented a hydrogen-dependent dislocation mobility law where the velocity of a screw dislocation is increased in the presence of hydrogen. This law was calibrated atomistically using kinetic Monte Carlo simulations [40,41], and the increased mobility is attributed to hydrogen-promoted kink-pair nucleation in the near core region. Therefore, a hydrogen-dependent dislocation mobility law, to some extent, accounted for the effect of hydrogen residing near the dislocation core and allowed the effect of hydrogen on a microcantilever to be simulated at a realistic concentration. Hydrogen residing in the core will not only affect kink-pair formation and migration but also change the dislocation core energy profile, which is critical for dislocation line tension and near-field interactions. Sills and Cai [42] suggested introducing a solute-solute interaction energy term to the hydrogen stress formulation. In this way, an additional free energy contribution from the near-core regime is incorporated, and this can be approximated as a change in the core energy due to hydrogen. With this method, Sills and Cai [42] were able to observe the effects of hydrogen on a dislocation loop and a Frank-Read (F-R) source at realistic bulk concentrations. In particular, a large decrease in the activation stress of the F-R source was observed, indicating the importance of the hydrogen core contribution in the activation of dislocation sources.

The force acting on a dislocation can be partitioned into two parts [43]: the elastic force and the core force, due to the dislocation core energy E^c . Hydrogen modifies this core energy and so contributes an additional hydrogen core force. The hydrogen core contribution is key in hydrogen-junction interactions, where the dislocation self-force and short-range interactions are crucial. Hydrogen elastic shielding and hydrogen-dependent dislocation mobility contribute marginally to dislocation junction formation which is regarded as a quasistatic process. As a demonstration, we performed DDD simulations of junction formation at low concentrations (0–60 appm), considering these contributions, and observed practically no change in junction length in the presence of hydrogen; see Sec. IV B for further details. To capture the effect of hydrogen on dislocation junctions, the hydrogen core force needs to be incorporated. The approach proposed by Sills and Cai [42] is a viable one, but as they noted, the near-core contribution was based on the stress field derived from linear elasticity theory, and the nonlinear interatomic interactions at the dislocation core were neglected. These nonlinear effects should be incorporated, which can be achieved by calibrating the dislocation core energy in the presence of hydrogen with atomistic simulations.

The main goal of this work is to present discrete dislocation dynamics simulations utilizing atomistic-level data for the dislocation core energies with and without hydrogen as input and investigate any emergent influence on plasticity. We assume the hydrogen core force arises as a result of hydrogen lowering the dislocation core energy, which is calibrated based on first principles density functional theory (DFT) calculations for

bcc iron. We show that the effects of hydrogen on dislocation junctions are dominated by the hydrogen core force. This highlights the important role of dislocation core energy in dislocation reactions. This work depicts a more general picture of how dislocation reactions are influenced by a change in dislocation core energy, using hydrogen as a medium to trigger the change.

This paper is organized as follows: Section II presents the details of the calibration of the hydrogen core energy using DFT. Section III discusses the effects of the hydrogen modified core energy on dislocation junction formation in bcc iron, using a line tension model. Section IV implements a hydrogen core force in the DDD framework and employs it to study the influence of hydrogen on dislocation junction properties. A summary is presented in Sec. V.

II. ATOMIC CALIBRATION

The line energy, E , of a dislocation can be partitioned into two parts [43],

$$E = E^e + E^c, \quad (1)$$

the elastic energy E^e and the core energy E^c . E^e can be calculated with linear elasticity theory whereas E^c is the energy contained within the dislocation core, typically within $5b$ from the dislocation line, where b is the magnitude of the Burgers vector. In an isotropic crystal, the elastic energy per unit length of a straight dislocation line is

$$E^e = \frac{\mu b^2}{4\pi(1-\nu)} \ln\left(\frac{R}{r_c}\right) (1 - \nu \cos^2 \theta), \quad (2)$$

μ is the shear modulus, ν is Poisson's ratio, R and r_c are the outer and inner cutoff radii, and θ is the character angle between the dislocation's Burgers vector and line direction. Material parameters for iron are used in this work: $a = 2.856 \text{ \AA}$ is the lattice parameter, $\mu = 82 \text{ GPa}$, and $\nu = 0.29$. Core energies in bcc Fe were determined in Refs. [44–46], which obtained values of $E_s^c = 0.219 \text{ eV/\AA}$ for a $1/2\langle 111 \rangle$ screw, $E_e^c = 0.286 \text{ eV/\AA}$ for a $1/2\langle 111 \rangle\{1\bar{1}0\}$ edge, and $E_c^c = 0.62 \text{ eV/\AA}$ for a $\langle 100 \rangle$ edge dislocation, calculated with core radii r_c , of 3, 2.45, and 5.16 \AA , respectively. We will notionally divide the hydrogen atoms into those which are trapped at distances greater than the core radius and usually referred to as forming an “atmosphere,” and those which occupy deep traps within the dislocation core. In the case of the hydrogen in the atmosphere, these occupy sites that we will assume to be equivalent to sites in an undistorted tetrahedral interstice and since these sites are not regular tetrahedra the associated strain is not purely dilatational. According to calculations using the density functional theory [47], the strain field of a single hydrogen atom in bcc Fe is

$$\epsilon^H = \begin{bmatrix} \epsilon_{11}^H & 0 & 0 \\ 0 & \epsilon_{22}^H & 0 \\ 0 & 0 & \epsilon_{33}^H \end{bmatrix} = \begin{bmatrix} 0.014 & 0 & 0 \\ 0 & 0.041 & 0 \\ 0 & 0 & 0.041 \end{bmatrix}. \quad (3)$$

The interaction energy per unit dislocation length, between a hydrogen in the atmosphere and a straight dislocation can then be determined following the continuum approach developed

in Ref. [48]. The interaction energy is

$$E^b(r) = a^3 \sum_{ij} \sigma_{ij}(r) \varepsilon_{ij}^H, \quad (4)$$

where a is the lattice constant and σ_{ij} is the stress field generated by the straight dislocation expressed in the same coordinate system as ε^H . The total interaction energy per unit dislocation length between the hydrogen atmosphere and a straight dislocation is

$$E^H(\chi_0) = \int_0^{2\pi} \int_{r_H}^{R_H} C_{\max} \chi(\varphi, r) E^b(\varphi, r) r dr d\varphi, \quad (5)$$

where r_H and R_H are the inner and outer cutoff radii of the hydrogen atmosphere centered at the dislocation. χ_0 is the nominal number of hydrogen atoms per iron atom; the concentration of hydrogen in atomic parts per million (appm) is thereby $c_0 = 10^6 \chi_0$. C_{\max} is the maximum solute concentration for the solid (in solutes per unit volume), and $\chi \equiv C/C_{\max}$ is the fraction of available lattice sites that are occupied by hydrogen [42].

Turning now to the hydrogen atoms trapped within the core, their binding energies, E^b , can be calculated using atomistic simulations [49,50]. These show that $1/2\langle 111 \rangle\{1\bar{1}0\}$ edge dislocations generate seven inequivalent hydrogen trap sites in the plane perpendicular to the dislocation line, with binding energies more negative than -0.1 eV (one with binding energy $E_1^b = -0.34$ eV, two with binding energies $E_2^b = -0.40$ eV, $E_3^b = -0.27$ eV, $E_4^b = -0.12$ eV). We note that magnetism is included in the calculated trap energies since these are taken from calculations within the local spin density approximation to the density functional theory [49]. The effect of trapped hydrogen is to reduce the dislocation line tension by the amount

$$G^H(\chi_0) = \sum_i \chi_i^b(\chi_0) E_i^b, \quad (6)$$

where the sum is over all the binding sites i along the dislocation line. The probability that a trap site is occupied by hydrogen is calculated from the McLean isotherm [51–53],

$$\chi_i^b = \frac{\frac{1}{6} \chi_0 \exp(E_i^b/k_B T)}{1 + \frac{1}{6} \chi_0 \exp(E_i^b/k_B T)}, \quad (7)$$

where the factor $1/6$ accounts for there being six tetrahedral sites per iron atom. The McLean equation expresses the dynamic equilibrium established at temperature, T , between hydrogen atoms dissolved in tetrahedral interstices and those trapped at defect sites i having a potential energy E_i^b . Alternatively interpreted, it describes the distribution of hydrogen that dictates that the chemical potential of hydrogen is constant across the microstructure. It is a valid approximation if we allow that hydrogen diffusion is the fastest of all the processes under consideration in the simulation [33,37]. The change in dislocation core energy per unit length, $E^{c,H}(\chi_0)$, is then

$$E^{c,H} = \frac{1}{L} G^H(\chi_0), \quad L = \begin{cases} \sqrt{6}a & \text{edge} \\ \sqrt{3}a/2 & \text{screw} \end{cases}, \quad (8)$$

where L is the periodic spacing along the dislocation line. The hydrogen concentration that we use in this work ranges between zero and 60 appm; typical concentrations found in

industrial applications are 1–10 appm, whereas specimens charged in the laboratory may reach 100 appm. In this range, the contribution to the total hydrogen-dislocation interaction energy from the near-core deep binding sites dominates. For instance, for a $1/2\langle 111 \rangle\{1\bar{1}0\}$ edge dislocation with $c_0 = 30$ appm, the contribution to the total binding energy per unit dislocation length due to “core” hydrogen calculated from Eq. (6) is 0.153 eV/Å, while the far-field elastic energy calculated from Eq. (5) with inner cutoff radius $r_H = a$ and outer cutoff radii $R_H = 100a$ and $R_H = 1000a$ are respectively 1.8 and 2.2 meV/Å. Apparently, divergence of the total energy with increasing outer cutoff radius R_H is very slow. We take $R_H = 100a$ for subsequent discussions, and we further approximate the total hydrogen binding energy as the hydrogen core energy. In the case of the $1/2\langle 111 \rangle$ screw dislocation, we use the deep near-core hydrogen binding sites calculated in Ref. [49]. Because the strain field is purely deviatoric in linear elasticity, the change in energy due to the hydrogen atmosphere is smaller than for the edge dislocation. In contrast to $1/2\langle 111 \rangle$ dislocations, the binding behavior of hydrogen atoms at the core of $\langle 100 \rangle$ dislocations has not been studied in detail with atomistic methods. Therefore, we determine the interaction energy between hydrogen and a straight $\langle 100 \rangle$ dislocation following the continuum approach [Eq. (5)] developed in Ref. [48]. As an approximation, we require the continuum approach [Eq. (5)] to yield the atomistically calibrated binding energy. Under this condition, the inner cutoff radius we determine at $c_0 = 30$ appm is $r_H = 0.435a$ for a $1/2\langle 111 \rangle$ edge dislocation. We further assume that the inner cutoff radius r_H determined for a $1/2\langle 111 \rangle$ edge dislocation also holds for a $\langle 100 \rangle$ edge dislocation. We then calculate the interaction energy of the hydrogen atmosphere and a $\langle 100 \rangle$ straight edge dislocation following Eq. (4), with the stress and strain fields provided in Ref. [54].

The core interaction energies, $E^{c,H}$, as functions of nominal hydrogen concentration, c_0 are shown in Fig. 1. The hydrogen core energy is negative and so will reduce the total core energy and total core force. It is noted that the magnitude of hydrogen core energies predicted for edge dislocations

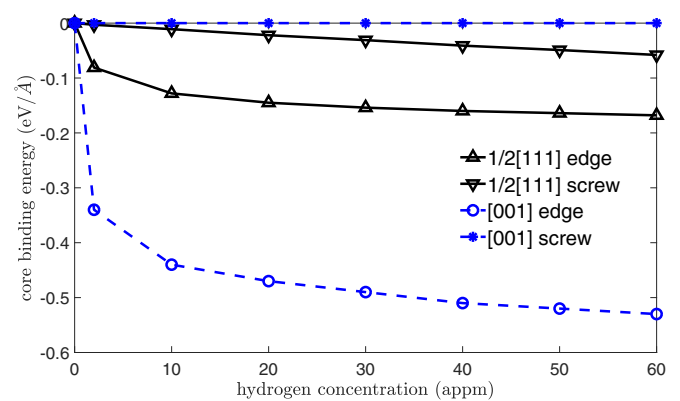


FIG. 1. The calibrated hydrogen core energy for $1/2\langle 111 \rangle$ and $\langle 100 \rangle$ dislocations. The hydrogen core energy is negative and so will reduce the total core energy and total core force. We refer to this as *hydrogen core force shielding*, as it is analogous to hydrogen elastic shielding [7].

agrees with the dislocation trap binding energies commonly seen in the literature [55]. It is also noted that the hydrogen binding energy for a $1/2\langle 111 \rangle$ screw dislocation is nonzero. This is because hydrogen has a tetragonal misfit strain which couples with the shear field of the $1/2\langle 111 \rangle$ screw dislocation to produce a nonzero interaction energy. In contrast, the hydrogen binding energy for a $\langle 100 \rangle$ screw dislocation is zero, because the hydrogen misfit strain does not couple with the elastic field in this case.

When two dislocation segments attract and intersect to form a junction, the dislocation lines rotate, resulting in a change in the angles between the Burgers vectors and line directions (the character angle, θ). The change in the character angle leads to rearrangement of hydrogen atoms around the dislocation which changes the interaction energy. The continuum method [Eq. (5)] can be used to calculate the interaction energy between the hydrogen atmosphere and a mixed straight dislocation. However, the inner cutoff radius depends on the character angle in reality, so accurate determination of the core interaction energy between hydrogen and a mixed dislocation is not feasible with the continuum approach without using reliable data for the inner cutoff radius, r_H , as a function of the character angle. In this study, we approximate the interaction energy $E(\theta)$ between a hydrogen atmosphere and a mixed $1/2\langle 111 \rangle$ dislocation segment with a character angle θ as an interpolation between the interaction energies $E_s^{c,H}$ and $E_e^{c,H}$ for the screw and edge segments calculated atomistically. $E_e^{c,H}$ has an approximately sinusoidal dependence on θ , and so the interpolation function in Refs. [42] and [56] is used,

$$E^{c,H} = E_e^{c,H} \sin^2 \theta + E_s^{c,H} \cos^2 \theta. \quad (9)$$

This interpolation is not unique; any number of schemes which enable a smooth transition from $E^{c,H}(0) = E_s^{c,H}$ to $E^{c,H}(\pi/2) = E_e^{c,H}$ could be used. We tested other interpolation schemes, including a linear interpolation, in the line tension model, and found that the influence of the interpolation scheme on dislocation junction formation is limited.

The atomic calibration presented in this section is based on certain simplifications and assumptions. A continuum approach was used for the $\langle 100 \rangle$ case. This was due to a lack of atomistic data in the literature on hydrogen binding to $\langle 100 \rangle$ dislocations in bcc metals. The key features of the hydrogen binding energy profile are that (i) the binding energy is more negative for edge than screw dislocations; (ii) the binding energy is small but nonzero for a $1/2\langle 111 \rangle$ screw and zero for a $\langle 100 \rangle$ screw; and (iii) a $\langle 100 \rangle$ edge dislocation possesses a more negative hydrogen binding energy than a $1/2\langle 111 \rangle$ edge dislocation. Point (iii) requires further discussion, since the core energy for a $\langle 100 \rangle$ edge dislocation was determined from an approximate continuum analysis. This trend is, however, physically reasonable as the $\langle 100 \rangle$ edge dislocation has a significantly higher core energy and produces more severe lattice distortion [57], providing more energetically favorable sites for hydrogen. Although hydrogen binding to $\langle 100 \rangle$ dislocations has not been reported in the literature, the binding behavior of carbon, also an interstitial solute, to $1/2\langle 111 \rangle$ and $\langle 100 \rangle$ dislocation loops in bcc iron has been investigated in several atomistic studies. According to Refs. [58,59], the binding energy is more than 50% more negative for $\langle 100 \rangle$ compared to $1/2\langle 111 \rangle$ dislocations. As

shown in Fig. 1, the hydrogen binding energy of a $\langle 100 \rangle$ edge dislocation is predicted by continuum elasticity to be over twice that for a $1/2\langle 111 \rangle$ edge dislocation. The exact $\langle 100 \rangle$ edge binding energy could differ from the continuum prediction, but it should still be larger in magnitude than the $1/2\langle 111 \rangle$ edge binding energy.

In the following sections, we employ the core energies in Fig. 1, but to examine how sensitive the results are to the $\langle 100 \rangle$ edge binding energy, a parametric study was also performed and is provided in the Appendix. We observe the same trends in behavior as reported below. The main effect of reducing the $\langle 100 \rangle$ edge binding energy is to decrease the length and strength of binary junctions (Fig. 14), while remaining larger than the hydrogen-free values. The screw triple junction is, however, insensitive to the variation of the $\langle 100 \rangle$ edge binding energy.

III. LINE TENSION MODEL OF JUNCTION FORMATION

To investigate the role of hydrogen trapped in the dislocation core on the formation of dislocation junctions, we investigate the intersection between straight dislocations moving on different glide planes. Our aim here is to evaluate hydrogen core effects on dislocation reactions and ignore the external stress and elastic interactions between dislocations. In bcc materials, both binary and triple junctions are important in plasticity [10]. Binary junctions result from the interaction of two dislocations on different slip systems and can influence the yield stress and early stages of work hardening, whereas triple junctions result from the interaction of three dislocations and are important during the late stages of work hardening. Triple junctions are strong anchors for dislocation entanglements and are potentially important in the formation of dislocation cell structures [10].

The binary junction geometry is illustrated in Fig. 2. Consider two straight dislocation line segments, with Burgers vectors b_1 and b_2 . Both segments are bound by a pair of pinning points.

The dislocation segments are in the slip planes with normals n_1 and n_2 and intersect at their midpoint, which is on the line of intersection of the two slip planes, $L = n_2 \times n_1 = [001]$. The dislocations are at angles ϕ_1 and ϕ_2 to L . A junction (a straight dislocation segment along L) with a Burgers vector $b_3 = b_1 + b_2$ will form if it reduces the energy of the system. If E_1 , E_2 , and E_3 are respectively the line energies of the reacting dislocations and junction, a junction will form if the following criterion is fulfilled [60]

$$E_1 \cos \phi_1 + E_2 \cos \phi_2 > E_3. \quad (10)$$

The energy of the configuration is a minimum when the condition

$$E_1 \cos \psi_1 + E_2 \cos \psi_2 - E_3 = 0 \quad (11)$$

is satisfied with equilibrium angles ψ_1 and ψ_2 , as illustrated in Fig. 2(b).

In order to evaluate the effect of hydrogen on junction formation, we consider the interaction between two $1/2\langle 111 \rangle$ edge dislocations, namely $1/2[1\bar{1}1](110)$ and $1/2[\bar{1}\bar{1}\bar{1}](1\bar{1}0)$, as illustrated in Fig. 2. The dislocations are of length $l_1 = l_2 = 200b$, and initially intersect at their midpoint.

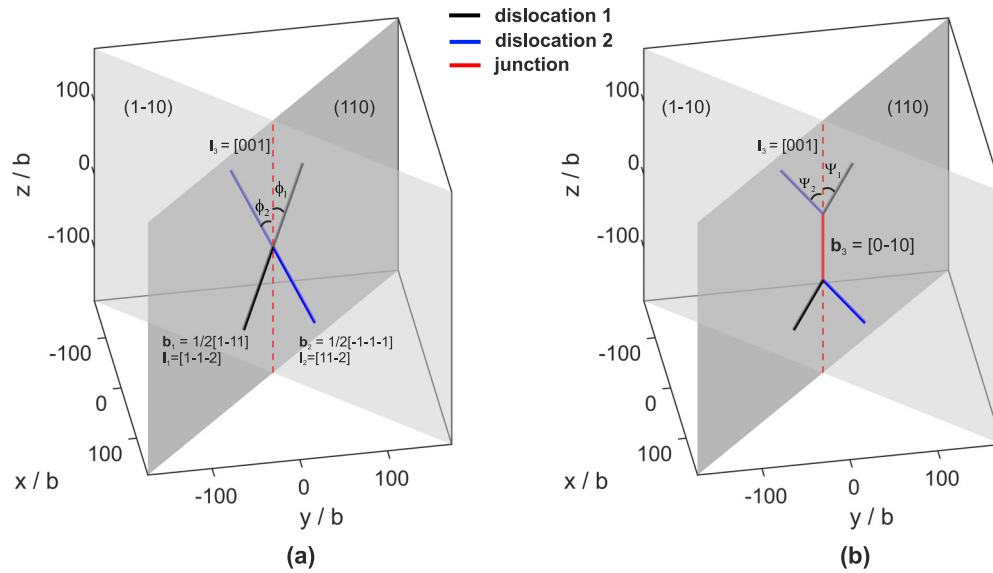
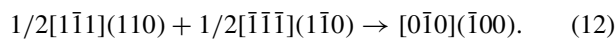


FIG. 2. Illustration of the binary junction geometry: (a) the initial configuration and (b) the junction formed after relaxation. The initial dislocations and the junction are of pure edge type.

The dislocations attract each other and their intersection results in an $[0\bar{1}0](\bar{1}00)$ edge junction:

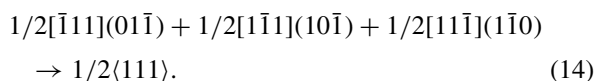


After including the dislocation core energy change due to hydrogen $E^{c,H}$ (shown in Fig. 1) into Eq. (1), the energy per unit dislocation length in the presence of hydrogen is

$$E = E^e + E^c + E^{c,H}. \quad (13)$$

To evaluate the elastic contribution to the dislocation energy, Eq. (2) is used, with $r_c = 3 \text{ \AA}$ for a $1/2\langle 111 \rangle$ screw dislocation, $r_c = 2.45 \text{ \AA}$ for a $1/2\langle 111 \rangle$ edge dislocation, and $r_c = 5.16 \text{ \AA}$ for a $\langle 100 \rangle$ dislocation; the outer cutoff radius is selected as $R = 100a$. As discussed in Sec. II, the far-field elastic energy due to hydrogen is neglected. To evaluate the effect of hydrogen on the dislocation reaction, at different bulk hydrogen concentrations, we determine the junction length which minimizes the energy of the configuration; by substituting the energies determined in Sec. II into Eq. (11). The calculations show an increase in binary junction length but almost no change in the triple junction length due to hydrogen. Since a $\langle 100 \rangle$ edge dislocation generates deeper binding sites (compared to a $1/2\langle 111 \rangle$ edge segment), the junction generated by the reaction traps more hydrogen atoms, reducing the energy of the system, and increasing the equilibrium binary junction length, as shown in Fig. 3.

In the triple junction case, we adopt the same configuration as in Ref. [10]. Three $\langle 111 \rangle\{\bar{1}\bar{1}0\}$ edge dislocations intersect at their midpoint and a $1/2\langle 111 \rangle$ screw-type triple junction is formed,



In this case, hydrogen atoms released during the reduction of the lengths of the reacting edge dislocations increases the energy of the configuration, and the magnitude of this is larger

than the energy reduction caused by hydrogen atoms binding to the screw junction. This leads to a reduction in the final screw junction length with hydrogen, as shown in Fig. 3. This reduction is very slight, since the energy change due to hydrogen is small compared to the total energy change during the formation of the triple junction.

The line tension model is a static approach for evaluating hydrogen core effects on dislocation reactions. It is applicable only for straight dislocation segments, while the external stress and dislocation interactions are ignored. In reality, under an applied stress, the dislocation segments will bow out. To study the effects of hydrogen on the intersection of curved dislocations requires including both the long-range elastic interaction due to hydrogen and the short-range interaction between dislocations and hydrogen at the core. Discrete dislocation dynamics (DDD) simulations on the effects of hydrogen on dislocation junctions are performed subsequently

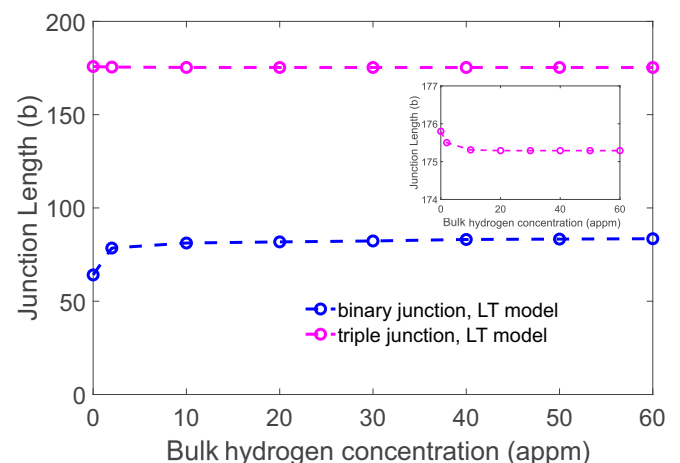


FIG. 3. Variation of junction length with hydrogen concentration calculated via the line tension (LT) model.

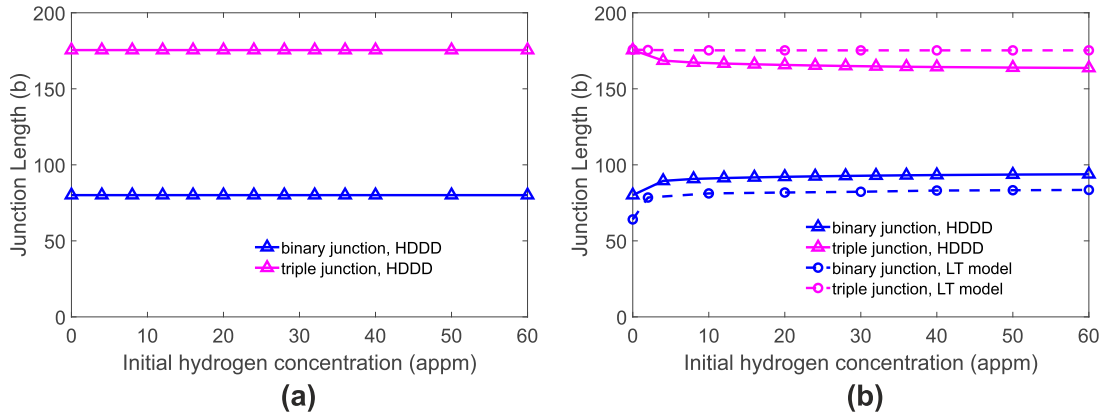


FIG. 4. (a) Variation of junction length with hydrogen concentration calculated via DDD without considering hydrogen core force shielding and (b) with hydrogen core force shielding.

for this purpose. Furthermore, DDD can be used to determine the junction strength, which is not possible with the line tension model.

IV. DDD SIMULATION WITH HYDROGEN CORE FORCE

Hydrogen influences dislocation plasticity by exerting elastic shielding and core force shielding and modifying the dislocation mobility. Long-range hydrogen elastic shielding and a hydrogen-dependent mobility law were implemented in Ref. [37]. However, the model was not able to capture the effect of hydrogen on dislocation junction formation, due to the short-range and quasistatic nature of the process. To some extent, this was implied in our recent work on the influence of hydrogen on Lomer junctions [30], where unrealistically high bulk concentrations were required for hydrogen to influence junction formation in the absence of hydrogen core effects. DDD simulations of binary and triple junctions are performed here, considering only hydrogen elastic shielding and a hydrogen-dependent mobility. The initial dislocation configurations are the same as for the line tension model in Sec. III. As shown in Fig. 4(a), the effect of hydrogen on junction length is not captured at these low concentrations. Comparison to the line tension model results (Fig. 3) indicates that hydrogen core force shielding dominates in the influence of hydrogen on junction formation.

A. Formulation

In the DDD simulation, dislocations are represented by discrete straight segments. The dislocation nodal velocity V_k is determined by balancing the drag force with the nodal driving force F_k on node k at position X_k . The nodal force is evaluated based on the nonsingular continuum theory of dislocations developed by Ref. [34]. In general, it consists of five parts in the presence of hydrogen

$$\begin{aligned} \mathbf{F}_k &= \sum_l \left(\sum_{i,j} \tilde{\mathbf{f}}_{kl}^{ij} + \sum_{i,j} \tilde{\mathbf{J}}_{kl}^{ij} + \mathbf{f}_{kl}^c + \mathbf{f}_{kl}^{c,H} + \hat{\mathbf{f}}_{kl} \right) \\ &= \tilde{\mathbf{F}}_k + \bar{\mathbf{F}}_k + \mathbf{F}_k^c + \mathbf{F}_k^{c,H} + \hat{\mathbf{F}}_k, \end{aligned} \quad (15)$$

where $\tilde{\mathbf{f}}_{kl}^{ij} = \tilde{\mathbf{f}}_{kl}^{ij}(X_k)$ is the interaction force at node k , due to segment $i \rightarrow j$ integrated along segment $k \rightarrow l$; this is summed over all segments $i \rightarrow j$ inside the domain, including the self-force due to segment $k \rightarrow l$, this is then summed over all nodes l which are connected to node k . Similarly, $\tilde{\mathbf{J}}_{kl}^{ij} = \tilde{\mathbf{J}}_{kl}^{ij}(X_k)$ is the hydrogen elastic shielding force evaluated at node k , implemented following the formulation proposed by Ref. [33]. $\mathbf{f}_{kl}^c = \mathbf{f}_{kl}^c(X_k)$ is the dislocation core force and $\mathbf{f}_{kl}^{c,H} = \mathbf{f}_{kl}^{c,H}(X_k)$ is the hydrogen core shielding force (that is missing in previous simulations). $\hat{\mathbf{f}}_{kl} = \hat{\mathbf{f}}_{kl}(X_k)$ is the corrective elastic force for the finite boundary value problem, which is evaluated with the finite element method using the superposition principle [61]. An underlying assumption of this formulation is that hydrogen is always in chemical equilibrium with dislocation stress field, which is also adopted in the calibration of hydrogen core energies. This is valid if hydrogen moves faster than dislocations which can be easily satisfied in bcc Fe [33] provided the stress is not too high $[\tau < (B/b)\sqrt{D/\Delta t} \approx (10^{-4}/10^{-10})\sqrt{10^{-4}/10^{-10}} \sim 1 \text{ GPa}]$.

In the presence of hydrogen, the core energy is

$$\begin{aligned} E_{\text{eff}}^c(\theta) &= E^c(\theta) + E^{c,H}(\theta) = E^c(\theta) - |E^{c,H}(\theta)| \\ &= \sin^2 \theta (E_e^c - |E_e^{c,H}|) + \cos^2 \theta (E_s^c - |E_s^{c,H}|), \end{aligned} \quad (16)$$

where E_e^c and E_s^c are the edge and screw dislocation core energies in the absence of hydrogen and $E_e^{c,H}$ and $E_s^{c,H}$ are the hydrogen core binding energies presented in Fig. 1. Note that the hydrogen core binding energies are negative, and therefore, hydrogen reduces the core energy of dislocations. The core force in the presence of hydrogen is then

$$\mathbf{f}_{kl}^c + \mathbf{f}_{kl}^{c,H} = E_{\text{eff}}^c(\theta) \mathbf{l}_{kl} + \frac{dE_{\text{eff}}^c(\theta)}{d\theta} \begin{pmatrix} \mathbf{b}_{kl}^e \\ |\mathbf{b}_{kl}^e| \end{pmatrix}, \quad (17)$$

where θ is the angle between \mathbf{l}_{kl} the line direction and Burgers vector of segment $k \rightarrow l$ with length L_{kl} . \mathbf{b}_{kl}^e is the edge component of the Burgers vector. This is the core force on dislocation node k due to its connection to node l , derived based on the core force being the first derivative of the total core energy of the discretized dislocation network with respect to the nodal positions. Further details can be found in Refs. [43] and [42]. The first term on the right-hand side

acts along the line direction to shrink the segment, while the second term is a moment tending to rotate the segment to the orientation with lowest core energy; in the absence of hydrogen this is the screw orientation. As discussed in Sec. II, different dislocation core radii and hydrogen free core energies were used for the $1/2\langle 111 \rangle$ and $\langle 100 \rangle$ dislocations in the atomistic calibration. To be consistent, the dislocation types were detected during the DDD simulation and assigned the core radii and hydrogen free core energies accordingly. For $1/2\langle 111 \rangle$ dislocations, a core radius of 3 \AA was used [44], whereas a core radius of 5.16 \AA was used for $\langle 100 \rangle$ dislocations [46]. In this way, the dislocation elastic energy and core energy are fully accounted for. Hu *et al.* [56] pointed out that the application of the core cutoff radius in conventional DDD modeling overlooks a considerable amount of elastic energy in the region between the real core radius and the cutoff radius used when evaluating the nonsingular elastic fields. To solve this issue, they extrapolated back from the cutoff radius to the real core radius and added the missing part of the elastic energy to the core energy term in the DDD simulation. Here, an equivalent result is achieved by setting the core cutoff radius in the DDD simulations equal to the core radius used in our atomistic calculations so that no elastic energy is omitted. It is noted that the core radius for $1/2\langle 111 \rangle$ edge dislocations should be 2.45 \AA , while the same core radius of 3 \AA was used for all $1/2\langle 111 \rangle$ dislocations for the ease of implementation in DDD. This slightly underestimates the elastic energy [Eq. (2)] of $1/2\langle 111 \rangle$ edge dislocations, but the difference is less than 5%. The hydrogen-free core energies for $1/2\langle 111 \rangle$ edge and screw dislocations are respectively $E_e^c = 0.286 \text{ eV/\AA}$ and $E_s^c = 0.219 \text{ eV/\AA}$ [44,45]; for $\langle 100 \rangle$ edge dislocation the value is $E_e^c = 0.62 \text{ eV/\AA}$ [46]. To the best of our knowledge, the dislocation core energy for $\langle 100 \rangle$ screw dislocation in iron has not been reported in the literature; therefore, the core energy for this case is approximated assuming $E_s^c = (1 - \nu)E_e^c = 0.44 \text{ eV/\AA}$. The atomistically determined core energies in the $1/2\langle 111 \rangle$ cases also follow this relation ($0.219/0.286 = 0.766 \approx 1 - \nu$). The validity of the treatment of dislocation core radii and energies is verified in Fig. 4(b), where good agreement is achieved in predicting the hydrogen-free junction lengths using the two different methods: the line tension model and DDD. This implementation of the hydrogen core force in [Eq. (17)] is applicable to other materials, provided the hydrogen core binding energies are properly calibrated.

A linear dislocation mobility law [37,43] is used. For each segment kl , a drag tensor \mathbf{B}_{kl} is determined according to the segment character, the nodal velocity \mathbf{V}_k at node k is then obtained using

$$\left[\frac{1}{2} \sum_l L_{kl} \mathbf{B}_{kl} \right]^{-1} \mathbf{F}_k = \mathbf{V}_k, \quad (18)$$

where the sum is over all nodes l connected to node k , and \mathbf{F}_k is the nodal force determined with Eq. (15). The mobility of a dislocation segment is anisotropic with respect to glide and climb and line, for example, an edge segment drag tensor has the form

$$\mathbf{B}_{kl} = B_g(\mathbf{m}_{kl} \otimes \mathbf{m}_{kl}) + B_c(\mathbf{n}_{kl} \otimes \mathbf{n}_{kl}) + B_l(\mathbf{l}_{kl} \otimes \mathbf{l}_{kl}), \quad (19)$$

where B_g and B_c are the drag coefficients for glide and climb, respectively. The unit vectors are the plane normal \mathbf{n}_{kl} and glide direction \mathbf{m}_{kl} . Full details are in Ref. [43]. The dislocation mobility is inversely proportional to the drag coefficient. In bcc materials, the mobility of a pure edge segment should be greater than that of a pure screw segment, which is accounted for by assigning $B_{eg} < B_s$. In the absence of hydrogen, the edge and screw drag coefficients are $B_{eg} = 5 \times 10^{-4} \text{ Pa s}$ and $B_s = 1 \times 10^{-2} \text{ Pa s}$ as used by Wang and Beyerlein [62]. The glide drag coefficient for a mixed segment is determined by interpolation between the screw and edge values using

$$B_g = [B_{eg}^{-2} \sin^2(\theta) + B_s^{-2} \cos^2(\theta)]^{-1/2}. \quad (20)$$

The drag coefficient for climb is set sufficiently high, $B_c = 1 \times 10^6 B_{eg}$, so that only glide occurs and the line drag coefficient is sufficiently low, $B_l = 1 \times 10^{-4} B_{eg}$, to allow nodes to move freely along the dislocation line.

Cross slip of screw segments is considered in a very simplified manner. For a screw segment, all possible cross-slip planes are checked and the plane with the maximum resolved shear stress is used as the cross-slip plane. The motion of the screw segment is then limited to this plane. For example, in the triple junction case, a $1/2\langle 111 \rangle$ screw junction is formed, whose possible cross-slip planes are the $(\bar{1}10)$, $(\bar{1}01)$, and $(0\bar{1}1)$ planes. Under uniaxial tension applied along $\langle 100 \rangle$, the screw junction will cross slip on the $(\bar{1}10)$ plane.

B. DDD modeling of dislocation junctions

1. Binary junction

The hydrogen elastic shielding and hydrogen-dependent mobility law were found to be unimportant over the range of concentrations considered here. Therefore, only hydrogen core force shielding is implemented unless stated otherwise.

Using the binary junction model in Sec. III, the effect of hydrogen on junction length is studied with DDD. The results are plotted against the line tension model predictions in Fig. 4(b). In contrast to Fig. 4(a), a significant hydrogen effect is captured, indicating the dominant role of hydrogen core force shielding in dislocation junctions. Good agreement is achieved between the DDD and line tension model. Some discrepancy is expected, as DDD accounts for the elastic interactions between segments, which is neglected in the line tension calculations.

A binary junction can be destroyed under an applied stress. The nonjunction segments can bow out, unzipping the junction and restoring the initial configuration. After a sufficient relaxation time, we apply a uniaxial tensile stress along $\langle 100 \rangle$. As the magnitude of the stress gradually increases, the junction will be unzipped, reducing the junction length. We take the stress σ_c at which the junction length first becomes zero as the strength of the binary junction. We simulate a hydrogen concentration of $c_0 = 10.0 \text{ appm}$. The initial dislocation length is varied from $l_0 = 200b$ to $l_0 = 800b$. The junction length and strength are shown in Fig. 5. Increasing the initial dislocation length increases the junction length (to obtain the equilibrium angles $\Psi_1 = \Psi_2 \approx 53.5^\circ$ without hydrogen and $\Psi_1 = \Psi_2 \approx 56.5^\circ$ with hydrogen) and reduces the

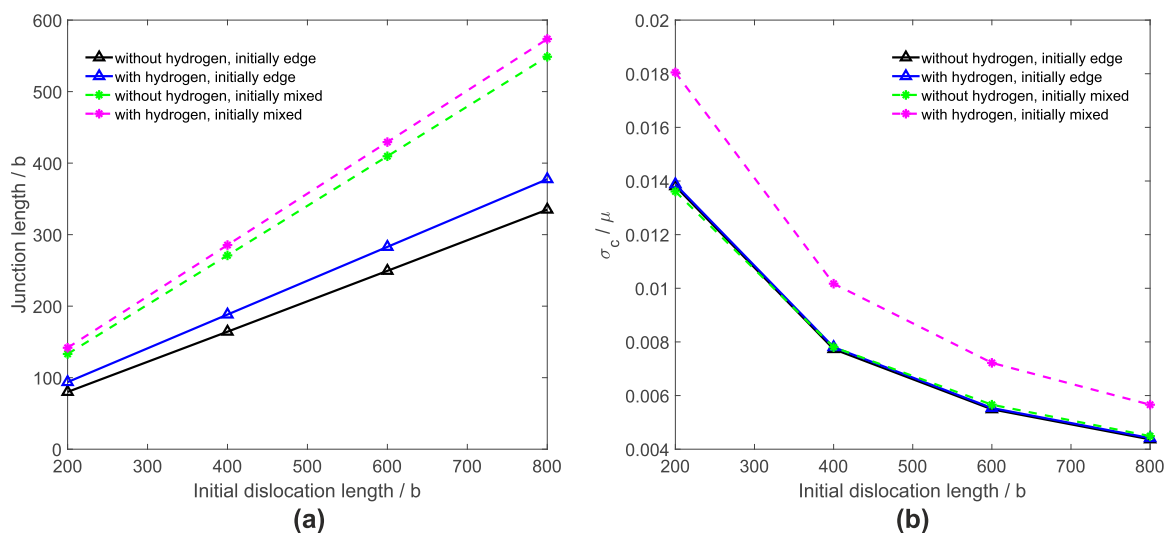


FIG. 5. The effect of hydrogen on binary junction (a) length and (b) strength.

junction strength. Consistent with the observation in Fig. 4, hydrogen increases the junction length, independently of the initial dislocation length. Hydrogen increases the strength of the junction for mixed initial segments and with initial edge segments the effect is negligible. The effect of hydrogen is dependent on the initial orientation of the intersecting dislocations, even if the line direction of the junction is fixed [30]. To be systematic, we rotated the initial dislocations inside their slip plane, changing their angles (ϕ_1, ϕ_2) with respect to the line direction of the junction ([001]); we tested all the cases with $\phi_1 = \phi_2$ and found that hydrogen increases the strength of the [001] junctions. A typical example with initially mixed segments at $\phi_1 = \phi_2 = 20^\circ$ is shown in Fig. 5.

It might be assumed that hydrogen increases the junction strength by increasing the junction length, thus shortening the initial segments and making it more difficult for them to bow out and unzip the junction. However, in Fig. 5(a), a large difference in junction length is observed between the two initial configurations in the absence of hydrogen;

in Fig. 5(b), however, the corresponding junction strengths are identical. This indicates the increase in junction strength due to hydrogen is not attributed to the hydrogen increased junction length but to some other mechanism.

The driving force for dislocation motion is partitioned into the hydrogen core force shielding term, $F^{c,H}$, and the hydrogen free forces, $\tilde{F}_k + \hat{F}_k + F^c$, as shown in Fig. 6. Finite boundary conditions were not considered in the junction simulations so $\hat{F}_k = 0$ in Fig. 6(a) and only accounts for the uniformly applied stress in Fig. 6(b). During formation, hydrogen lowers the core energy of the $\langle 100 \rangle$ junction. The hydrogen core forces act to stretch the junction, reducing the total core force and increasing the junction length. The destruction of the junction is realised via a procedure similar to the operation of a F-R source. A $1/2\langle 111 \rangle$ arm which is pinned at one end and constrained to move along the line of the junction at the other end is activated and bows out, which drives the mobile node along the line, unzipping the junction. The hydrogen core force tends to impede the expansion of

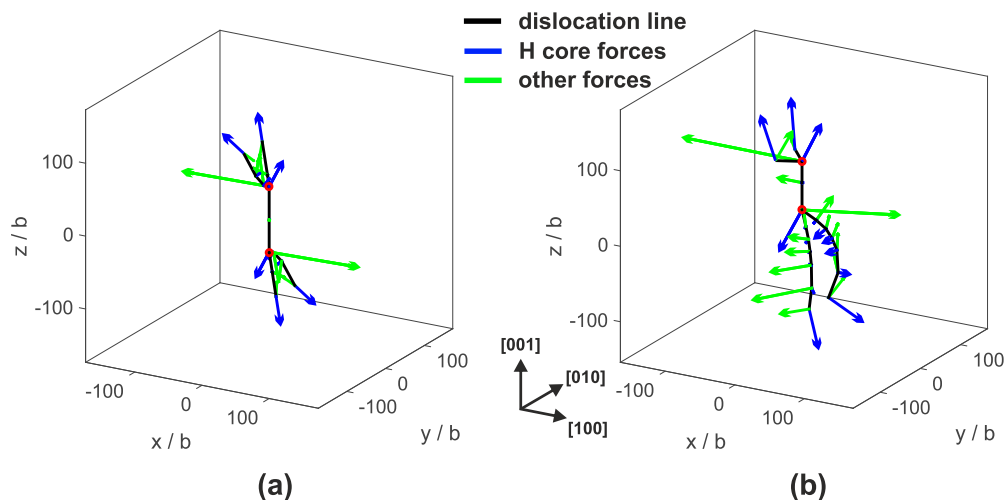


FIG. 6. The nodal force partitioned into hydrogen, $F^{c,H}$ (blue arrows), and nonhydrogen parts $\tilde{F}_k + \hat{F}_k + F^c$ (green arrows). (a) Formation (zipping) of a [001] junction. (b) Destruction (unzipping) of the junction. The end points of the junction are marked with red circles; note $F^{c,H}$ has been scaled $5\times$ for clarity.

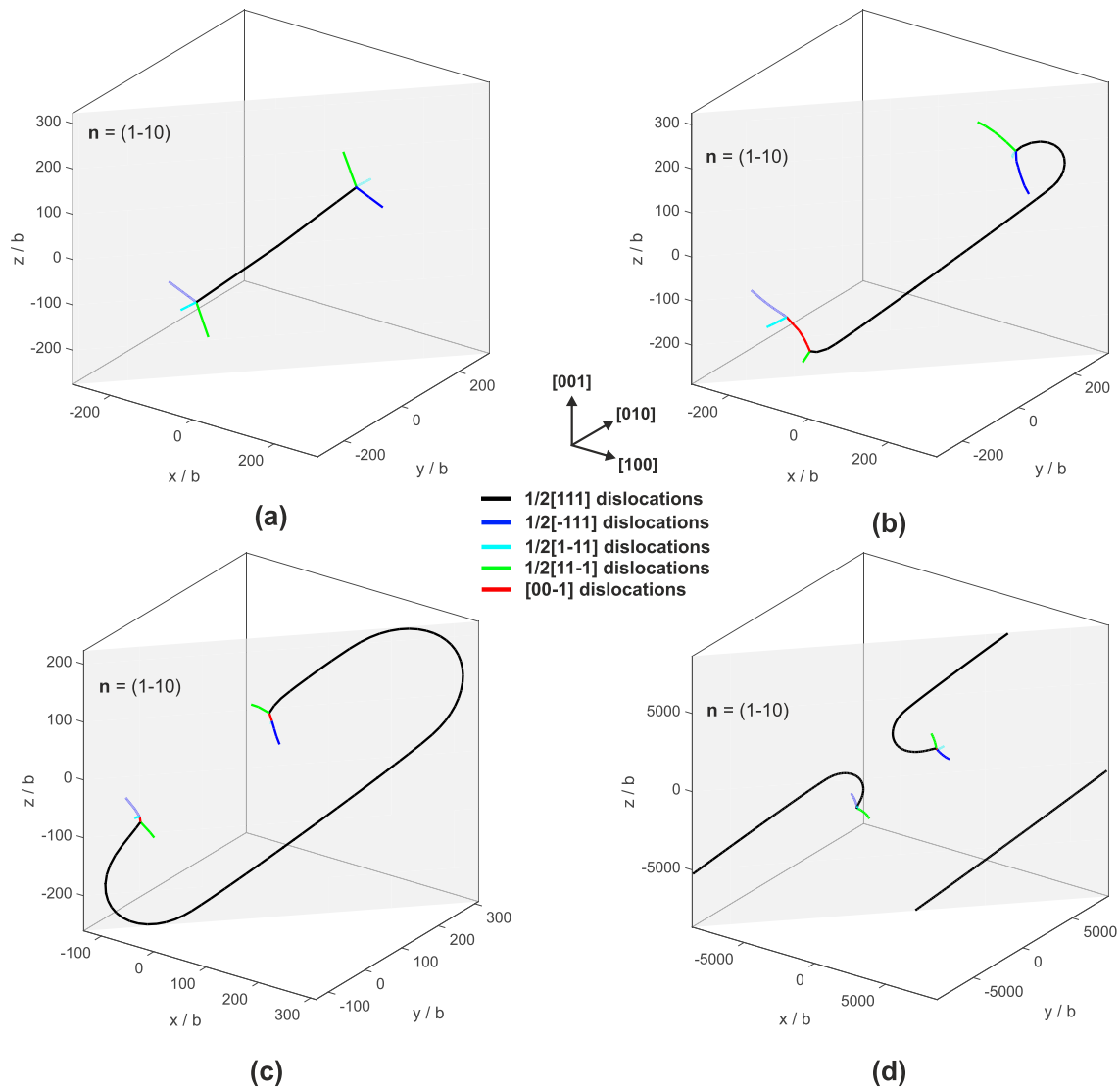


FIG. 7. A screw triple junction operating as a F-R source. (a) Initial triple junction before bow out; (b) Interaction between the $1/2\langle 111 \rangle$ (black) dislocation loop and the $1/2[11\bar{1}]$ (green) arm on the left, forming a $[00\bar{1}]$ sessile dislocation (red): $1/2[11\bar{1}](1\bar{1}0) + 1/2[\bar{1}\bar{1}\bar{1}](1\bar{1}0) \rightarrow [00\bar{1}](1\bar{1}0)$; (c) $1/2\langle 111 \rangle$ loop has bowed back, restoring the $1/2[11\bar{1}]$ arm, and the process then occurs on the right. (d) Moment just before the emission of a full loop, restoring the triple junction as in panel (a), and the process repeats.

this F-R source, making the destruction of the junction more difficult. Finally, it should be noted that the opposite was observed in fcc materials where hydrogen elastic shielding weakens Lomer junctions [30].

2. Triple junction

Triple junctions are stronger than binary junctions. In Ref. [10], the authors observed more pronounced strain hardening in the presence of triple junctions and attributed the phenomenon to the propensity of these junctions to form additional dislocation sources. Triple junctions occur at a late stage of loading, serving as strong anchors which form complex dislocation networks which impede dislocation motion. Unlike the $\langle 001 \rangle$ binary junctions, which are sessile, the $1/2\langle 111 \rangle$ triple junctions are glissile and considerably longer than the other $1/2\langle 111 \rangle$ arms. As a result, the junction (rather than the nonjunction segments) will bow out under an external

stress, meaning rather than unzipping, the junction operates like a F-R source.

Therefore, the strength of a triple junction is defined here as the stress required to nucleate a loop. After the pure screw triple junction is formed, out-of-plane pure shear is applied to one of its possible cross slip planes, the $(1\bar{1}0)$ plane, and the motion of the $1/2\langle 111 \rangle$ screw dislocation is limited to this plane.

When the applied stress is sufficiently high, the triple junction will bow out and generate dislocation loops, as shown in Fig. 7. This procedure is similar to the F-R operation but has some unique features which have not been discussed before. On each of the possible cross-slip planes (i.e., the possible F-R operation planes), there lie a pair of $1/2\langle 111 \rangle$ arms formed during the relaxation process. The bowing-out loop will inevitably interact with one of these pairs during the operation. In the case selected here, it is the $1/2[11\bar{1}]$ (green) pair. As shown in Fig. 7(b), the junction encounters

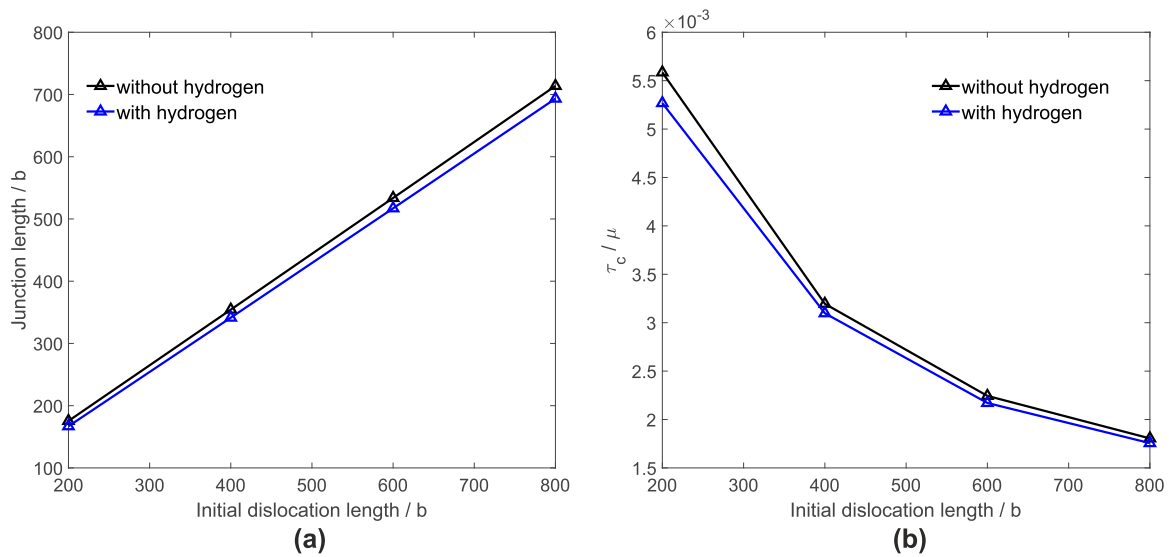


FIG. 8. Variation of (a) triple junction length and (b) strength with initial dislocation length, with and without hydrogen.

the arm on the left as soon as it bows out, which yields a sessile $[00\bar{1}]$ segment (red): $1/2[11\bar{1}](1\bar{1}0) + 1/2[\bar{1}\bar{1}\bar{1}](1\bar{1}0) \rightarrow [00\bar{1}](1\bar{1}0)$. Note that the line direction of the junction is opposite to the $1/2[11\bar{1}]$ arm when they first interact. This impedes the expansion of the loop on the left and leads to the asymmetric development of the loop as shown in Fig. 7(b). As expansion continues, the loop will eventually bypass the pinning point, bow sharply back, and wrap around the now sessile arm (red), restoring it back to its initial state (green): $[00\bar{1}](1\bar{1}0) + 1/2\langle 111 \rangle(1\bar{1}0) \rightarrow 1/2[11\bar{1}](1\bar{1}0)$. The same process, where a temporary sessile $[00\bar{1}]$ segment is formed, then occurs on the other pinning point, as shown on the right of Fig. 7(c).

During the activation of a F-R source and similarly of the triple junction, there exists a certain geometric configuration beyond which the dislocation line becomes unstable and keeps growing and emits loops. During the simulation, the magnitude of the applied stress is gradually increased until the triple junction starts to operate and reaches the critical geometry [42], and thus the critical activation stress τ_c , i.e., junction strength, is determined. We have verified that the predicted activation stresses obtained for pure screw F-R sources in the absence of hydrogen agree with the $\frac{3}{2}\mu b/L$ relation expected by theoretical calculation [54]. The formation length and destruction strength of the triple junctions of varying length with and without hydrogen ($c_0 = 10.0$ appm) are shown in Fig. 8. Consistent with the results in Fig. 4(b), the hydrogen core force slightly reduces the length and strength of the triple junction. However, the effect is negligible as it is a second-order effect. Hydrogen was observed to impede the bowing out of an edge dislocation, consistent with the solute drag mechanism [63]. This is in contrast to the results shown here; however, here we are looking at the bowing out of a screw dislocation subjected to steady-state hydrogen redistribution under constant chemical potential, while in Ref. [63] the initial hydrogen concentration was an order of magnitude higher and the total amount of hydrogen was constant during the simulation.

The nodal forces are shown in Fig. 9. In Fig. 9(a), the hydrogen core force tends to shrink the triple junction.

During the activation of the triple junction, as shown in Fig. 9(b), the hydrogen core force tends to enhance bowing out of the mixed dislocation segments while impeding the edge segments, which facilitates the bow out and nucleation of a loop. This accounts for the slight reduction in stress with hydrogen in Fig. 8(b). A hydrogen-dependent mobility law [37] was not incorporated in the current simulations. A significant enhancement in the operation of the triple junction/F-R source is expected if hydrogen-enhanced screw mobility is implemented.

It is hard to anticipate the consequence of hydrogen on the mechanical response by analysis of individual junctions. For this purpose, hydrogen-junction interactions should be discussed in the context of a complex dislocation network formed in a volume of material under an applied load.

C. Microcantilever simulation with hydrogen core force shielding

To examine if hydrogen core force shielding could affect mechanical properties, we performed DDD simulations of a microcantilever bend test. The beam is aligned along the $\langle 100 \rangle$ crystallographic axes and has dimensions of $12 \times 3 \times 3 \mu\text{m}$ with $\mathbf{u}(0, y, z) = [0, 0, 0]$, $\mathbf{u}(L_x, y, L_z) = [0, 0, U]$ with an applied displacement of $U = -0.08 \mu\text{m}$, and the remaining surfaces are traction free. Fully integrated linear brick finite elements, $0.24 \mu\text{m}$ in size, were used to solve for the corrective elastic fields at every time increment [37]. The initial dislocation structure consisted of 40 square prismatic loops with a length of $0.39 \mu\text{m}$ randomly generated from the three slip systems of interest in Eq. (14), $1/2[\bar{1}11](01\bar{1})$, $1/2[1\bar{1}1](10\bar{1})$, and $1/2[11\bar{1}](1\bar{1}0)$, positioned randomly in the high-stress region near the fixed end $x < 4 \mu\text{m}$. This enables the formation of binary junctions as well as triple and higher order junctions referred to here as multijunctions. A hydrogen concentration of 10 appm was applied when computing the core force, apart from this the simulations with and without hydrogen were identical. The evolution of the total dislocation density, together with the load-displacement

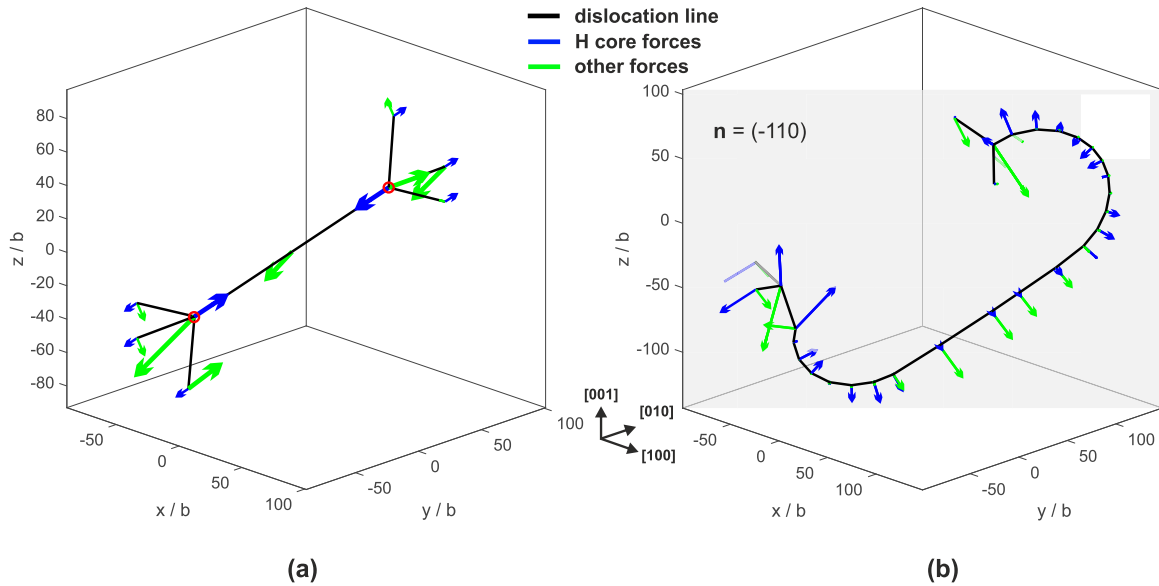


FIG. 9. The nodal force partitioned into hydrogen core force, $F^{c,H}$ (blue arrows), and nonhydrogen parts $\tilde{F}_k + \hat{F}_k$ (green arrows). (a) Formation of the triple junction. (b) Bow out of the junction. The ending points of the junction in panel (a) are marked with red circles; note $F^{c,H}$ has been scaled $20\times$ with respect to $\tilde{F}_k + \hat{F}_k$ for clarity.

curves, are plotted in Fig. 10. During the early loading stage ($30 < U < 70$ nm), the dislocation density is slightly higher in the presence of hydrogen and yielding seems to occur earlier with hydrogen, but the effect is not pronounced, compared to the hydrogen softening effect observed in Ref. [37], where hydrogen enhanced screw dislocation mobility was considered. This indicates that the influence of hydrogen core force shielding on yielding is limited but is important during dislocation interactions and junction formation.

The evolution of the binary and multijunction densities with and without hydrogen are shown in Fig. 11. During the entire loading history, binary junctions are the dominant junction type. The density of binary junctions is significantly higher in the presence of hydrogen, as shown in Fig. 11(a). This is consistent with hydrogen increasing the length and strength of binary junctions, as discussed earlier. In Fig. 11(b), hydrogen also increases the proportion of multijunctions,

which usually form when a mobile dislocation interacts with a binary junction to form a triple junction.

The increased junction density with hydrogen eventually reduces the mobile density production rate leading to subsequent hardening, as evident in Fig. 10(a) for $U > 0.07 \mu\text{m}$. This corresponds to the mobile density with hydrogen dropping below that without hydrogen. A snap shot (at $U = -0.0524 \mu\text{m}$) of the dislocation structure in the initial (hydrogen softening) stage is shown in Fig. 12. The $1/2[1\bar{1}1](10\bar{1})$ and $1/2[1\bar{1}1](1\bar{1}0)$ slip systems have the highest Schmid factor and so are the most active and make up the majority of the mobile density. The higher binary junction density (red) with hydrogen is also visible in Fig. 12(b).

The dislocation structure at the end of the simulation ($U = -90$ nm) is shown in Fig. 13. Figure 13(a), compared with Fig. 12(a), shows an increase in the mobile density (green and blue) in the absence of hydrogen. Comparing Fig. 13(b) with

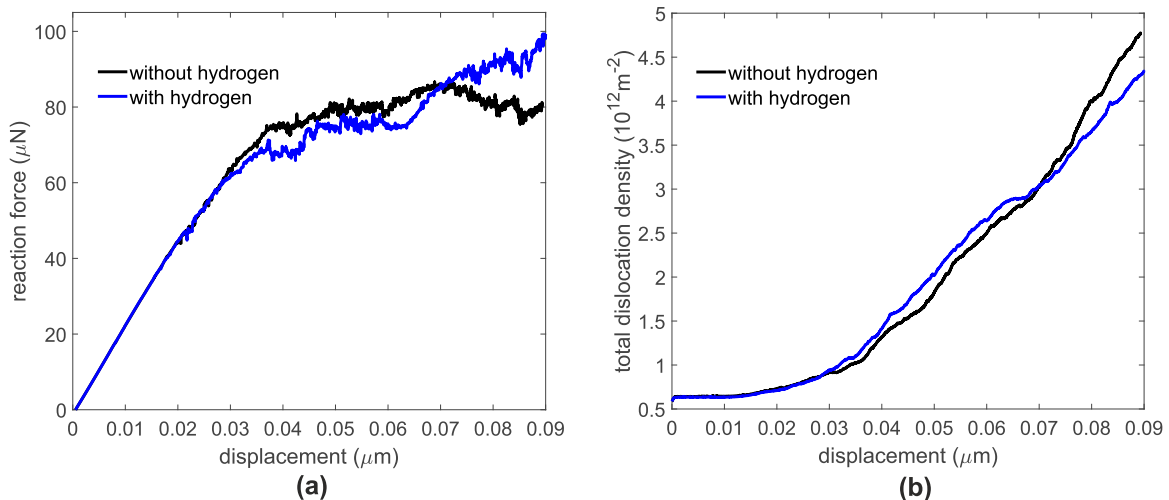


FIG. 10. (a) The load-displacement curve; (b) the evolution of the total dislocation density.

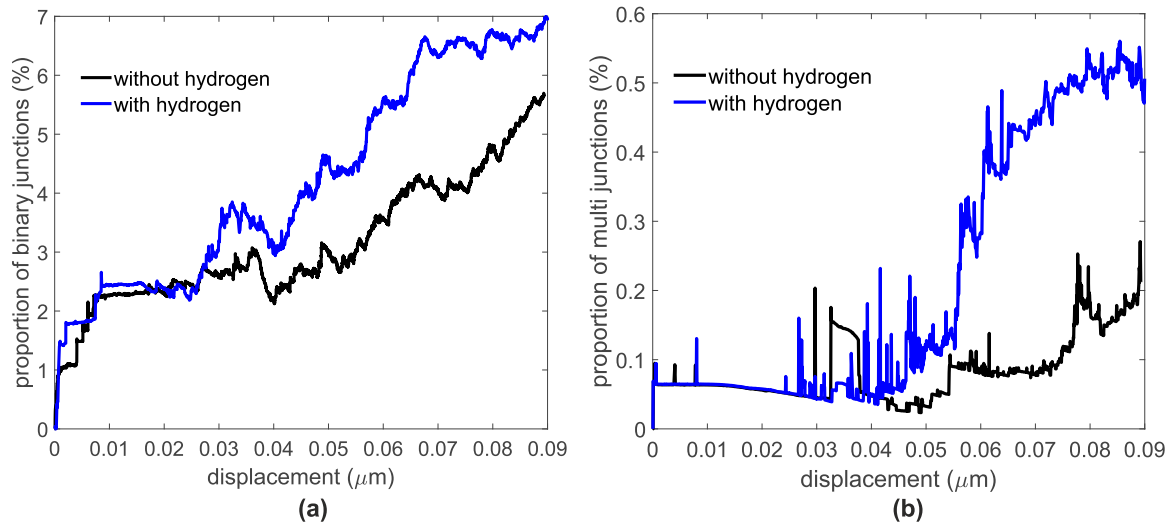


FIG. 11. (a) The evolution of binary dislocation junction density; (b) the evolution of multiple dislocation junction density.

Fig. 13(a) shows the higher junction density and lower mobile density with hydrogen.

Hydrogen significantly increases the density of junctions, leading to more complicated dislocation tangles, which will impede the motion of dislocations as loading increases. Therefore, hydrogen core force shielding is expected produce a hardening effect as loading increases. Recently, Wang *et al.* [64] observed that hydrogen increases strain hardening in an fcc twinning-induced plasticity (TWIP) steel and hydrogen hardening was observed in bcc iron, both experimentally [65] and numerically [66]. It should also be noted that the increased strain hardening mechanism revealed here is due to the interaction of hydrogen with dislocation junctions and is different from the solute strengthening mechanism based

on the bowing out of the F-R source like dislocations in Refs. [67,68].

In the future, we will simulate and interpret real micro-cantilever bend tests. However, the hydrogen-enhanced dislocation mobility, which is omitted here for clarity, should be taken into account and the specimen geometry should include a notch to initiate fracture, as is common experimentally [38].

V. SUMMARY

In this work, a hydrogen core force shielding mechanism was proposed; i.e., hydrogen “shields” the dislocation core force by decreasing the dislocation core energy. Atomic calibration and implementation of this mechanism in DDD

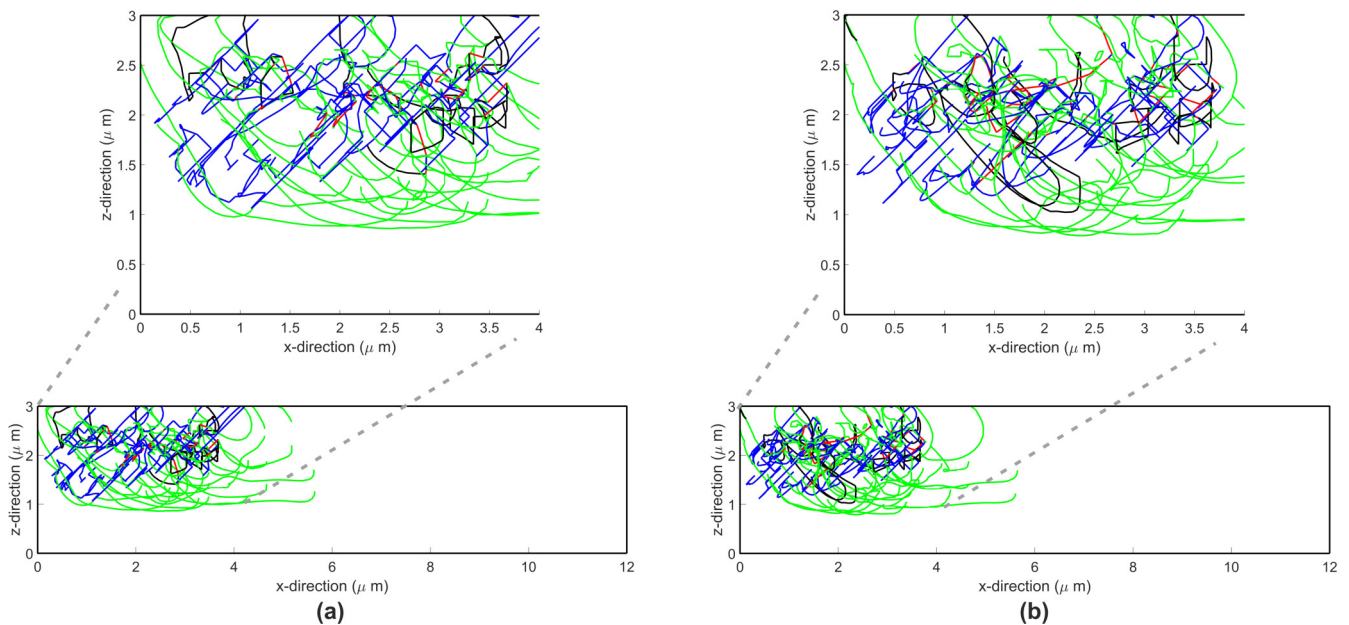


FIG. 12. Dislocation structure in the initial loading stage $U = -50$ nm: (a) without hydrogen and (b) with hydrogen. The dislocations belonging to the three initial slip systems are $1/2[\bar{1}11](01\bar{1})$ (black), $1/2[1\bar{1}1](10\bar{1})$ (blue), and $1/2[11\bar{1}](1\bar{1}0)$ (green) with binary junctions (red) and multiple dislocation junctions (magenta).

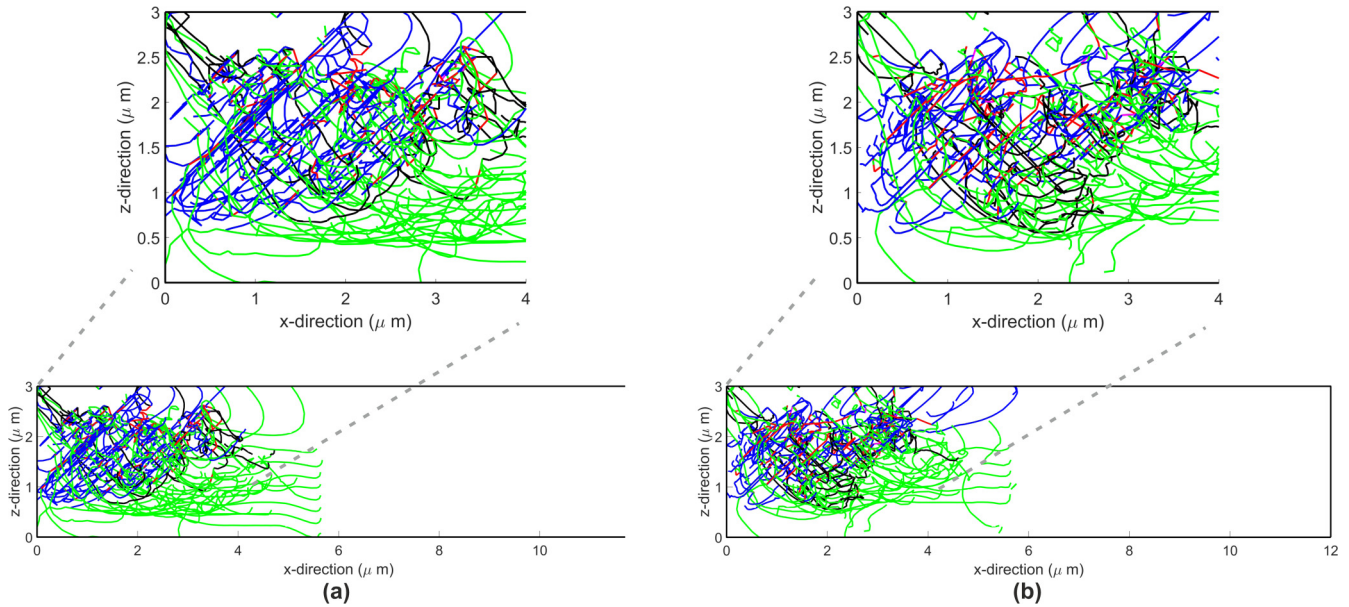


FIG. 13. Dislocation structure at $U = -90$ nm: (a) without hydrogen and (b) with hydrogen. With the same color coding as Fig. 12.

simulations were performed. The main conclusions are summarized below.

(1) With the hydrogen core force shielding mechanism, hydrogen-induced softening was reproduced at a realistic bulk concentration commonly seen in experiments. In contrast, no influence of hydrogen was predicted with the hydrogen elastic shielding mechanism at similar concentrations [37].

(2) Due to its short-range nature, the hydrogen core force shielding mechanism has a pronounced influence on the activity of dislocation junctions. Hydrogen was found to increase the length and strength of $\langle 100 \rangle$ binary edge junctions. For certain configurations, the enhancement in strength can be as much as 30%. The increased binary junction strength could lead to a significant increase in the number of junctions forming in large-scale simulations, limiting the motion of dislocations.

(3) In microcantilever plasticity simulations, the hydrogen core force shielding mechanism caused an increase in the density of dislocation junctions, resulting in an in-

crease in strain hardening visible in the load-displacement curve.

Other contributions such as the hydrogen effect on dislocation mobility [37] were not considered. In the future, larger scale DDD simulations should be performed to interpret experimental data and to inform larger scale crystal plasticity models incorporating hydrogen.

ACKNOWLEDGMENTS

This work was supported by the Engineering and Physical Sciences Research Council (EPSRC) under Programme Grant No. EP/L014742/1 and Fellowship Grant No. EP/N007239/1; I.H.K. acknowledges support from Bulgaria National Science Fund (BNSF) under Programme Grant No. KP-06-H27/19; H.Y. acknowledges Bruce Bromage for useful discussions.

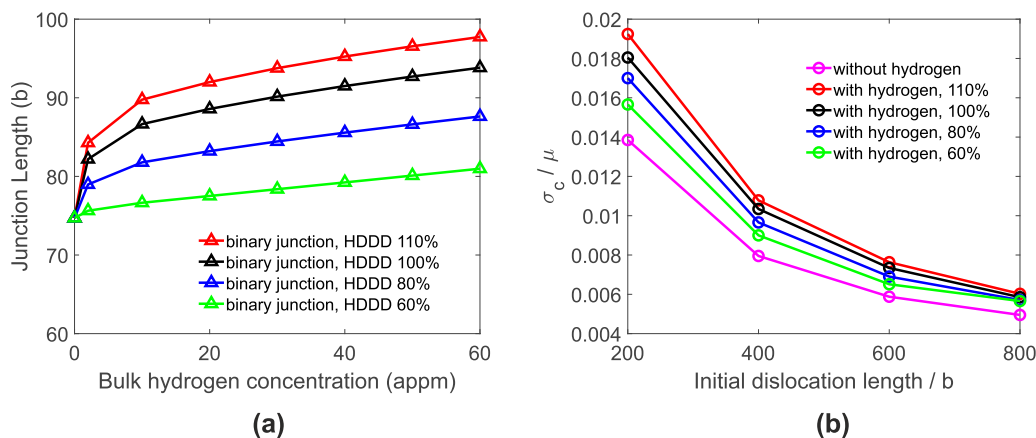


FIG. 14. Variation of the (a) length and (b) strength of binary junctions with different $\langle 100 \rangle$ binding energies. The three cases +10%, -20%, and -40% and the original case are shown. These figures correspond to Figs. 4(b) and 5(b), respectively.

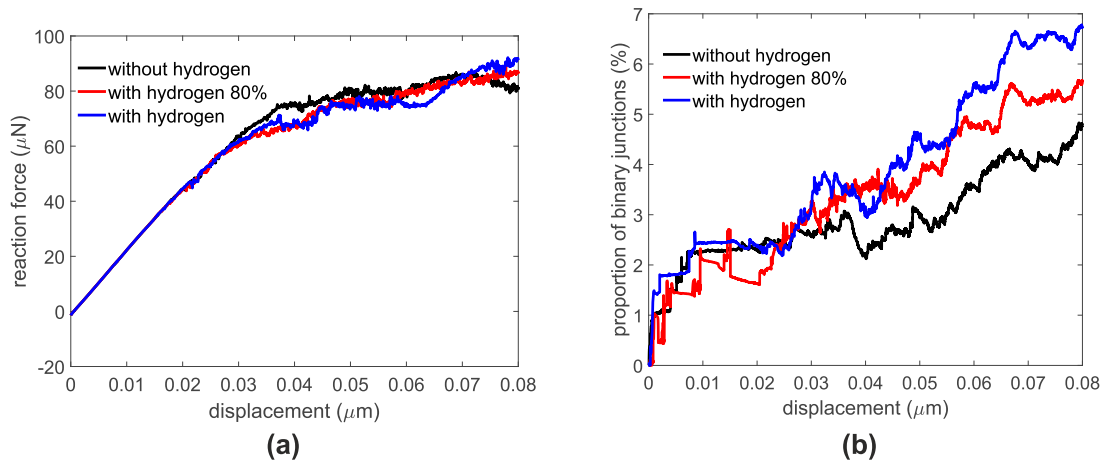


FIG. 15. (a) The load-displacement curves extracted from the microcantilever simulations; (b) the evolution of binary junction density during the loading of the microcantilevers. These figures correspond to Figs. 10(a) and 11(a), respectively.

APPENDIX: SENSITIVITY ANALYSIS WITH RESPECT TO VARIOUS $\langle 100 \rangle$ BINDING ENERGIES

A sensitivity study of the simulation results with respect to the $\langle 100 \rangle$ binding energy is required, since a continuum approach [Eq. (5)] of unknown accuracy was employed to determine the $\langle 100 \rangle$ binding energy. For this purpose, the $\langle 100 \rangle$ binding energy was varied and the junction formation and destruction simulations were repeated. The magnitude of the $\langle 100 \rangle$ edge binding energy should not fall below the $1/2\langle 111 \rangle$ edge binding energy, nor should it exceed the hydrogen free core energy of the dislocation. Based on these principles, three cases were selected, +10%, -20%, and -40% with respect to the original $\langle 100 \rangle$ binding energy curve calibrated in Fig. 1.

The binary junction length is sensitive to the variation in the $\langle 100 \rangle$ binding energy, as shown in Fig. 14. The theoretical calculation of binary junction length using the line tension model gives a picture very similar to Fig. 14(a) and so is

not presented. The binary junction length and strength are increased when hydrogen is present in all the cases analyzed. The extent of the strengthening is dependent on the magnitude of the $\langle 100 \rangle$ binding energy. Both the theoretical calculation and the DDD simulation show negligible change in the triple junction length and strength with the variation in the $\langle 100 \rangle$ binding energy (figures not presented here). This is because hydrogen has a limited effect on the triple junctions, as shown in Figs. 4(b) and 8(b).

The conclusions in the main text regarding the effects of hydrogen on microcantilever plasticity also hold qualitatively. The DDD simulation of a microcantilever is repeated with the $\langle 100 \rangle$ binding energy reduced by 20%. As shown in Fig. 15(b), the binary junction density is slightly reduced but still higher than the hydrogen free case, which is consistent with the observation in Fig. 14. The dislocation structure at the end of the simulation is very similar to that shown in Fig. 13(b) and is not presented here.

- [1] I. M. Robertson, *Eng. Fract. Mech.* **68**, 671 (2001).
- [2] T. Tabata and H. Birnbaum, *Scr. Metall.* **17**, 947 (1983).
- [3] I. M. Robertson and H. K. Birnbaum, *Acta Metall.* **34**, 353 (1986).
- [4] D. S. Shih, I. M. Robertson, and H. K. Birnbaum, *Acta Metall.* **36**, 111 (1988).
- [5] P. J. Ferreira, I. M. Robertson, and H. K. Birnbaum, *Acta Mater.* **46**, 1749 (1998).
- [6] P. J. Ferreira, I. M. Robertson, and H. K. Birnbaum, *Acta Mater.* **47**, 2991 (1999).
- [7] H. K. Birnbaum and P. Sofronis, *Mater. Sci. Engin. A* **176**, 191 (1994).
- [8] D. Delafosse, in *Gaseous Hydrogen Embrittlement of Materials in Energy Technologies*, Woodhead Publishing Series in Metals and Surface Engineering, Vol. 1, edited by R. P. Gangloff and B. P. Somerday (Woodhead Publishing Limited, Cambridge, UK, 2012), pp. 247–285.
- [9] N. Grilli, K. G. F. Janssens, J. Nellessen, S. Sandlöbes, and D. Raabe, *Int. J. Plast.* **100**, 104 (2018).
- [10] V. V. Bulatov, L. L. Hsiung, M. Tang, A. Arsenlis, M. C. Bartelt, W. Cai, J. N. Florando, M. Hiratani, M. Rhee, G. Hommes, T. G. Pierce, and T. D. de la Rubia, *Nature (London)* **440**, 1174 (2006).
- [11] S. Wang, N. Hashimoto, and S. Ohnuki, *Mater. Sci. Engin. A* **562**, 101 (2013).
- [12] X. L. Wu, Y. T. Zhu, Y. G. Wei, and Q. Wei, *Phys. Rev. Lett.* **103**, 205504 (2009).
- [13] L. Wang, X. Han, P. Liu, Y. Yue, Z. Zhang, and E. Ma, *Phys. Rev. Lett.* **105**, 135501 (2010).
- [14] J. H. Lee, T. B. Holland, A. K. Mukherjee, X. Zhang, and H. Wang, *Sci. Rep.* **3**, 1061 (2013).
- [15] M. S. Colla, B. Amin-Ahmadi, H. Idrissi, L. Malet, S. Godet, J. P. Raskin, D. Schryvers, and T. Pardoen, *Nat. Commun.* **6**, 5922 (2015).
- [16] V. Bulatov, F. F. Abraham, L. Kubin, B. Devincre, and S. Yip, *Nature (London)* **391**, 669 (1998).
- [17] V. Bulatov and W. Cai, *Computer Simulations of Dislocations* (Oxford University Press, Oxford, UK, 2006), Vol. 3.

- [18] D. Rodney and R. Phillips, *Phys. Rev. Lett.* **82**, 1704 (1999).
- [19] V. Yamakov, D. Wolf, S. R. Phillpot, and H. Gleiter, *Acta Mater.* **51**, 4135 (2003).
- [20] T. A. Parthasarathy and D. M. Dimiduk, *Acta Mater.* **44**, 2237 (1996).
- [21] R. Madec, B. Devincre, L. Kubin, T. Hoc, and D. Rodney, *Science* **301**, 1879 (2003).
- [22] E. Martínez, J. Marian, A. Arsenlis, M. Victoria, and J. M. Perlado, *J. Mech. Phys. Solids* **56**, 869 (2008).
- [23] R. Madec, B. Devincre, and L. P. Kubin, *Phys. Rev. Lett.* **89**, 255508 (2002).
- [24] H. M. Zbib, M. Rhee, and J. P. Hirth, *Int. J. Mech. Sci.* **40**, 113 (1998).
- [25] V. B. Shenoy, R. V. Kukta, and R. Phillips, *Phys. Rev. Lett.* **84**, 1491 (2000).
- [26] S.-W. Lee, S. Aubry, D. Nix, William, and W. Cai, *Modell. Simul. Mater. Sci. Eng.* **19**, 025002 (2011).
- [27] C.-C. Wu, S. Aubry, A. Arsenlis, and P. W. Chung, *Int. J. Plast.* **79**, 176 (2016).
- [28] R. G. Hoagland and M. I. Baskes, *Scr. Mater.* **39**, 417 (1998).
- [29] Q. Chen, X. Y. Liu, and S. B. Biner, *Acta Mater.* **56**, 2937 (2008).
- [30] H. Yu, A. C. Cocks, and E. Tarleton, *Scr. Mater.* **166**, 173 (2019).
- [31] G. M. Castelluccio, C. B. Geller, and D. L. McDowell, *Int. J. Plast.* **111**, 72 (2018).
- [32] K. Zhao, J. He, A. E. Mayer, and Z. Zhang, *Acta Mater.* **148**, 18 (2018).
- [33] Y. Gu and J. A. El-Awady, *J. Mech. Phys. Solids* **112**, 491 (2018).
- [34] W. Cai, A. Arsenlis, C. R. Weinberger, and V. V. Bulatov, *J. Mech. Phys. Solids* **54**, 561 (2006).
- [35] W. Cai, R. B. Sills, D. M. Barnett, and W. D. Nix, *J. Mech. Phys. Solids* **66**, 154 (2014).
- [36] Q. Song, Z. Li, Y. Zhu, and M. Huang, *Int. J. Plast.* **111**, 266 (2018).
- [37] H. Yu, A. Cocks, and E. Tarleton, *J. Mech. Phys. Solids* **123**, 41 (2019).
- [38] Y. Deng and A. Barnoush, *Acta Mater.* **142**, 236 (2018).
- [39] J. Song and W. A. Curtin, *Acta Mater.* **68**, 61 (2014).
- [40] I. H. Katzarov, D. L. Pashov, and A. T. Paxton, *Phys. Rev. Mater.* **1**, 033602 (2017).
- [41] There was an error in Ref. [40]. We employed a factor 1/3 rather than the correct factor 1/6 in the McLean isotherm (7). This means that all values of hydrogen concentration both in the text and in the figures should be multiplied by two to be corrected.
- [42] R. B. Sills and W. Cai, *Philos. Mag.* **98**, 1491 (2018).
- [43] A. Arsenlis, W. Cai, M. Tang, M. Rhee, T. Opperstrup, G. Hommes, T. G. Pierce, and V. V. Bulatov, *Modell. Simul. Mater. Sci. Eng.* **15**, 553 (2007).
- [44] E. Clouet, L. Ventelon, and F. Willaime, *Phys. Rev. Lett.* **102**, 055502 (2009).
- [45] E. Clouet, *Philos. Mag.* **89**, 1565 (2009).
- [46] Y. Zhang, L.-J. Xie, J.-M. Zhang, and K.-W. Xu, *Chin. Phys. B* **20**, 026102 (2011).
- [47] S. Wang, K. Takahashi, N. Hashimoto, S. Isobe, and S. Ohnuki, *Scr. Mater.* **68**, 249 (2013).
- [48] A. W. Cocharadt, G. Schoeck, and H. Wiedersich, *Acta Metall.* **3**, 533 (1955).
- [49] M. Itakura, H. Kaburaki, M. Yamaguchi, and T. Okita, *Acta Mater.* **61**, 6857 (2013).
- [50] H. Kimizuka and S. Ogata, *Phys. Rev. B* **84**, 024116 (2011).
- [51] D. McLean, *Grain Boundaries in Metals* (Clarendon Press, Oxford, UK, 1957).
- [52] E. D. Hondros and M. P. Seah, *Metall. Trans. A* **8**, 1363 (1977).
- [53] M. Guttman and D. McLean, in *Interfacial Segregation*, edited by W. C. Johnson and J. M. Blakely (American Society of Metals, OH, 1979), pp. 261–348.
- [54] P. Anderson, J. Hirth, and J. Lothe, *Theory of Dislocations* (Cambridge University Press, Cambridge, UK, 2017).
- [55] C. Ayas, J. A. W. van Dommelen, and V. S. Deshpande, *J. Mech. Phys. Solids* **62**, 113 (2014).
- [56] Y. Hu, B. Szajewski, D. Rodney, and W. Curtin, *Modell. Simul. Mater. Sci. Eng.* **28**, 015005 (2019).
- [57] M. R. Fellingner, A. M. Z. Tan, L. G. Hector, Jr., and D. R. Trinkle, *Phys. Rev. Mater.* **2**, 113605 (2018).
- [58] D. Terentyev, N. Anento, and A. Serra, *J. Nucl. Mater.* **420**, 9 (2012).
- [59] D. Terentyev, N. Anento, and A. Serra, *J. Phys.: Condens. Matter* **24**, 455402 (2012).
- [60] J. D. Baird, B. Gale, and N. P. Allen, *Philos. Trans. Royal Soc. London, Ser. A* **257**, 553 (1965).
- [61] E. V. d. Giessen and A. Needleman, *Modell. Simul. Mater. Sci. Eng.* **3**, 689 (1995).
- [62] Z. Q. Wang and I. J. Beyerlein, *Int. J. Plast.* **27**, 1471 (2011).
- [63] A. Tehrani and W. A. Curtin, *Eng. Fract. Mech.* **216**, 106502 (2019).
- [64] D. Wang, X. Lu, Y. Deng, X. Guo, and A. Barnoush, *Acta Mater.* **166**, 618 (2019).
- [65] T. Depover, E. Wallaert, and K. Verbeken, *Mater. Sci. Engin. A* **664**, 195 (2016).
- [66] W. Xie, X. Liu, W. Chen, and H. Zhang, *Comput. Mater. Sci.* **50**, 3397 (2011).
- [67] G. P. M. Leyson, W. A. Curtin, L. G. Hector, and C. F. Woodward, *Nat. Mater.* **9**, 750 (2010).
- [68] G. P. M. Leyson, L. G. Hector, and W. A. Curtin, *Acta Mater.* **60**, 3873 (2012).